

## Chapter 8

# Visible Signatures from Hidden Sectors

### 8.1. Introduction

In this section we discuss a broad class of models with visible signatures due to the presence of hidden gauge symmetries. The specific classes of models we review each have a hidden sector, a visible sector and a communication between the hidden and the visible sectors. While there are many hidden sector models which have been discussed, we will focus here on communication via Stueckelberg mass mixing [1,2,3,4], higher dimension operators mediated by heavy states in Hidden Valleys [5,6,7,8], models with mediation via kinetic mixing [9,10,11,4,12,13] and specifically kinetic mixing in the class of dark force models discussed in [14,15,16,17]. We also discuss generalized portals occurring due to hidden-visible sector couplings arising from both kinetic and mass mixings [4,18,19].

The concept of the hidden sector has a long history and its modern roots lie in supersymmetry where hidden sectors are responsible for the breaking of supersymmetry. However, typically the fields in the hidden sectors are very massive. Thus while the consequences of the hidden sectors have direct bearing on the building of phenomenologically viable models whose experimental signatures will be probed at the LHC and in dark matter experiments, the actual internal dynamics of the hidden sector are unreachable directly with colliders or cosmology. However, more recently it has been shown that hidden sectors can give rise to unique signatures at colliders when

the mass scale in the hidden sector is well below a TeV, as in Hidden Valleys, Stueckelberg extensions and Unparticle models. In particular, confining dynamics in the hidden sector [5,6,20,21] give rise to exotic signatures such as high jet multiplicity events [8] and lepton jets, and such events multiplicities are also a feature of the models of Refs. [14,15,16,17]. Thus in models with extended hidden sectors, the cascades and dynamics can become rich and complex. Rich event topologies arise in models of Stueckelberg mass generation and kinetic mixings, where multi-lepton jet signals and missing energy are a consequence of gauged hidden sector vector multiplets. Here one has complex susy cascades and heavy flavor jet signatures from new scalars [2], multilepton production and jet production [3,4,22] as well as the possibility of mono-jet and mono-photon signatures [23]; where the latter signatures also arise in the models of [24,25,16].

There are indeed many recent developments in hidden sector models, and by no means will we be able to cover all models, which include Higgs mediators, light gauged mediators and axion mediators, see e.g., [11,26,23,4,27,28,18,19,29,24,13,12,14,15,30,31,33,32], as well as investigations of their phenomenological implications [34,35,36,37,16,17,38,39,40,41,42,25,43,44,45,46,47,48,22]. We aim instead to outline some of the possibilities, and refer the reader to these references for further details.

These classes of models also lead to astrophysi-

cal predictions offering several explanations to the recent positron anomaly seen in the PAMELA satellite data. Such proposals include multi-component dark matter [31], a boost in positrons from a sommerfeld enhancement [14] and a Breit-Wigner enhancement of dark matter annihilations [32] (see also [4]). Further, the presence of hidden sector states degenerate with the dark matter particle can lead instead to a boost in the relic density via coannihilation effects [26,22]. We discuss now some of the models in further detail.

## 8.2. Stueckelberg Extensions

### 8.2.1. Massive Stueckelberg vector bosons

The Stueckelberg mechanism allows for mass generation for a  $U(1)$  vector field without the benefit of a Higgs mechanism. The  $U(1)_X$  Stueckelberg extensions of the Standard Model (SM)[1], i.e.,  $SU(3)_C \times SU(2)_L \times U(1)_Y \times U(1)_X$ , involve a non-trivial mixing of the  $U(1)_Y$  hypercharge gauge field  $B^\mu$  and the  $U(1)_X$  Stueckelberg field  $C^\mu$ . The Stueckelberg field  $C^\mu$  has no couplings with the visible sector fields, while it may couple with a hidden sector, and thus the physical  $Z'$  gauge boson connects with the visible sector only via mixing with the SM gauge bosons. These mixings, however, must be small because of the LEP electroweak constraints[3].

The  $U(1)_X$  Stueckelberg extension of the Standard Model (SM) can be generalized further to include a gauge kinetic mixing (StkSM)[4]. In the gauge vector boson sector, the effective Lagrangian is then given by  $\mathcal{L}_{\text{StkSM}} = \mathcal{L}_{\text{SM}} + \Delta\mathcal{L}$  [4]

$$\begin{aligned} \Delta\mathcal{L} \ni & -\frac{1}{2}(\partial_\mu\sigma + M_1 C_\mu + M_2 B_\mu)^2 \quad (8.1) \\ & -\frac{1}{4}C_{\mu\nu}C^{\mu\nu} - \frac{\delta}{2}C_{\mu\nu}B^{\mu\nu} + g_X J_X^\mu C_\mu \end{aligned}$$

where  $\delta$  is the gauge kinetic mixing parameter and  $M_1, M_2$  are the Stueckelberg mass parameters [4,18,19]. Here  $\sigma$  is a pseudoscalar axion which transforms under  $U(1)_X$  as well as under  $U(1)_Y$  so that  $\Delta\mathcal{L}$  is gauge invariant.

Upon coupling to the SM, the HS and VS mix through the neutral vector boson sector and one finds a massless photon  $A$ , the  $Z$  boson, and

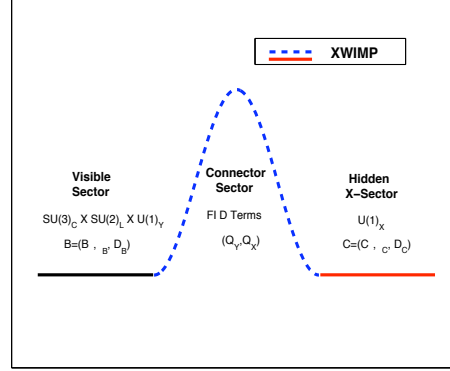


Figure 8.1. An XWIMP contains a combination of fields both from the VS and the HS which communicate due to the presence of a connector sector (CS). Suppressed interactions in the HS leads to a boost in the relic density relative to what would be obtained without the presence of the HS states[26,22]. (Figure from [26]).

a  $Z'$  boson, the latter of which is dominantly composed of  $C$ . In the *absence* of kinetic mixing, this arises from diagonalizing the mass<sup>2</sup> matrix in the neutral vector sector (in the basis  $(C, B, A^3)_\mu$ ) [1,2,3]

$$\begin{bmatrix} M_1^2 & M_1^2\epsilon & 0 \\ M_1^2\epsilon & M_1^2\epsilon^2 + \frac{1}{4}v^2g_Y^2 & -\frac{1}{4}v^2g_2g_Y \\ 0 & -\frac{1}{4}v^2g_2g_Y & \frac{1}{4}v^2g_2^2 \end{bmatrix}, \quad (8.2)$$

where the effective parameter is the ratio  $\epsilon \equiv M_2/M_1$ , which is constrained by the electroweak data such that  $|\epsilon| \lesssim 0.061\sqrt{1 - (M_Z/M_1)^2}$ . This constraint was derived in [3] and a very similar constraint appears in the Refs(1,2) of [11]. Consequently the couplings of the  $Z'$  boson to the visible matter fields are extra weak, leading to a very narrow  $Z'$  resonance when decays to hidden sector matter are forbidden[1,3]. The physical width of such a boson could be as wide as  $\mathcal{O}(100 \text{ MeV})$  or as narrow as a few MeV or even narrower and lie in the sub-MeV range [3], provided that the  $Z'$  does not decay into hidden sector matter [23]. These widths are much smaller than those that arise for the  $Z$  primes in GUT models (see Ref. [6]) for a recent review of  $Z'$  models, as well as an overview of other models

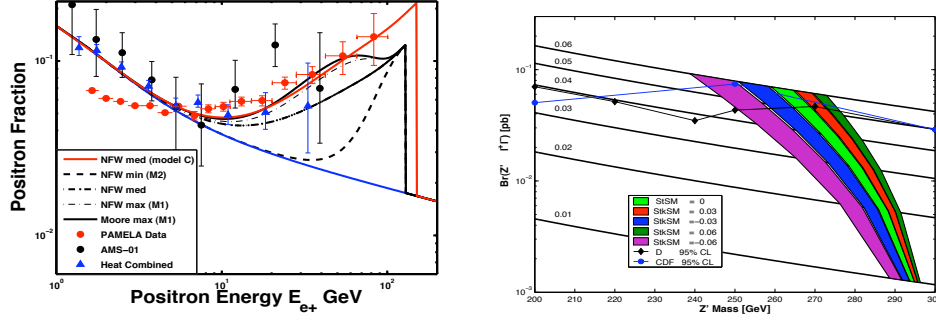


Figure 8.2. Left: A dark Dirac fermion ( $m_D$ ) which couples to the Stueckelberg  $Z'$  produces fits to the PAMELA positron data [49] due to the presence of a Breit-Wigner Pole [4]. Right: The Stueckelberg  $Z'$  produces a detectable signal in the dilepton channel consistent with electroweak constraints (black curves) and simultaneously produced the correct relic abundance of dark matter in the vicinity of the Breit-Wigner Pole [3] (shaded/colored bands). The Stueckelberg  $Z'$  can therefore be tested at low mass ranges where  $Z'$  from GUT models are already eliminated [3,50].

with Stueckelberg mass mixing [52,53]). In the presence of kinetic mixing along with Stueckelberg mass mixing but with no matter fields in the hidden sector, it is shown in [4] that the analysis of the electroweak sector depends not on  $\epsilon$  and  $\delta$  separately but on the rescaled parameter  $\bar{\epsilon} = (\epsilon - \delta)/(1 - \delta^2)^{1/2}$  and it is therefore  $\bar{\epsilon}$  that is constrained rather than  $\epsilon$  by the electroweak data. However, in the presence of matter in the hidden sector the analysis in the electroweak sector will depend both on  $\epsilon$  and on  $\delta$ . Further, it is easily seen that all matter in the hidden sector acquires a milli charge [1,3,23,4,28,36,37,43].

### 8.2.2. Explaining PAMELA Positron Data

The Dirac fermion in the hidden sector discussed above is a natural candidate for dark matter and explicit analyses show this to be the case [23,4]. Further, the recent PAMELA positron excess anomaly can be naturally explained by a Breit-Wigner enhancement of the annihilation cross sections of these Dirac fermions in the galaxy when they annihilate in the vicinity of the  $Z'$  pole. Such enhancement can only be achieved when  $M_{Z'} \lesssim 2M_D$  [32] where  $M_D$  is the mass of the Dirac fermion. This phenomenon is shown in Fig.(8.2). Thus, the interaction of the hidden sector matter with the Stueckelberg field given in [2] produces upon diagonalization

$g_X Q_X J_X^\mu C_\mu \rightarrow \bar{D} \gamma^\mu [c_A A_\mu + c_Z Z_\mu + c_{Z'} Z'_\mu] D$ , while  $c_{Z'}/c_Z \approx c_{Z'}/c_A \sim 30$  for  $\epsilon = .06$ ; i.e. for  $(Q_X, g_X) = (1, g_Y) \rightarrow c_{A,Z} \sim 1/100$ , while  $c_{Z'} \sim g_Y$ . One may then obtain the integrated cross section for  $\sigma(D\bar{D} \rightarrow f\bar{f})$  [23,4,32],

$$\sigma_{f\bar{f}} \simeq \frac{N_f s \beta_f}{32\pi \beta_D} [(|\xi_L|^2 + |\xi_R|^2) \cdot F_1 + Re(\xi_L^* \xi_R) \cdot F_2],$$

where  $F_1 = 1 + \beta_D^2 \beta_f^2 / 3 + 4M_D^2 s^{-1} (1 - 2m_f^2/s)$ ,  $F_2 = 8m_f^2 s^{-1} (1 + 2M_D^2/s)$ ,  $\beta_{f,D} = (1 - 4m_{f,D}^2/s)^{1/2}$ ,  $s = 4m_D^2/(1 - v^2/4)$  and  $\xi_{L,R}$  include the  $(\gamma, Z, Z')$  poles. The dominant effect in the mass range of interest arise from the Breit-Wigner  $Z'$  pole

$$\xi_{L,R}^{Z'} = \frac{C_D^{Z'} C_{fL,R}^{Z'}}{s - M_{Z'}^2 + i\Gamma_{Z'} M_{Z'}}$$

where the explicit expressions for the couplings are given in [4,32]. The Breit-Wigner enhancement allows for the satisfaction of the relic density consistent with the WMAP data as shown in Fig.(8.2).

### 8.2.3. Stueckelberg Extension of MSSM

The Stueckelberg extension of MSSM (StMSSM) is constructed from a Stueckelberg chiral multiplet mixing vector superfield multiplets for the  $U(1)_Y$  denoted by  $B = (B_\mu, \lambda_B, D_B)$

and for the  $U(1)_X$  denoted by  $C = (C_\mu, \lambda_C, D_C)$  and a chiral supermultiplet  $S = (\rho + i\sigma, \chi, F_S)[1,3]$

$$\mathcal{L}_{\text{St}} = \int d^2\theta d^2\bar{\theta} (M_1 C + M_2 B + S + \bar{S})^2. \quad (8.3)$$

The Lagrangian of Eq.(8.3) is invariant under the supersymmetrized gauge transformations:  $\delta_Y(C, B, S) = (0, \Lambda_Y + \bar{\Lambda}_Y, -M_2 \Lambda_Y)$  and  $\delta_X(C, B, S) = (\Lambda_X + \bar{\Lambda}_X, 0, -M_1 \Lambda_X)$ . In the above, the superfield  $S$  contains a scalar  $\rho$  and an axionic pseudo-scalar  $\sigma$ . The StMSSM model class also provides an example of a model where the astrophysical implications for a wino LSP (a wino LSP in the MSSM has been re-emphasized in [54,22]) as well as a mixed Higgsino wino LSP [22] have important effects on observables. A new feature of this extension (for technical details see [2,26,22]) is that it expands the neutralino sector of the MSSM. The neutralino sector consists of the Majorana spinors  $(\chi_1^0, \chi_2^0, \chi_3^0, \chi_4^0)$  and minimally new Majorana fields labeled  $(\xi_1^0, \xi_2^0)$  formed out of the  $U(1)_X$  gaugino and the chiral fermion from the chiral fields  $S$  and  $\bar{S}$ .

### 8.2.4. Enhancement of Relic Density via Coannihilation with Hidden Matter

We discuss now an interesting phenomenon in that matter in the hidden sector can coannihilate with the LSP which has the effect of enhancing the relic density for the LSP by as much an order of magnitude or more. This enhancement can occur through the presence of  $n$   $U(1)_X$  gauge symmetries in the hidden sector and  $n$  sets of new scalars with Stueckelberg masses generated for the  $n$   $U(1)_X$  gauge bosons[22]. This model then leads to  $2n+4$  Majorana states:  $(\chi_1^0, (\xi_1^0, \xi_2^0 \dots \xi_{2n}^0), \chi_2^0, \chi_3^0, \chi_4^0)$  where  $\chi_i^0$  ( $i = 1, 2, 3, 4$ ) are essentially the four neutralino states of the MSSM and  $\xi_\alpha^0$ , ( $\alpha = 1, \dots, 2n$ ) are the additional states [55]. Assuming that the Majorana fields of the hidden sector interact extra weakly, one finds that there is an enhancement of the relic density by a factor  $B_{Co}$  through coannihilation effects. This enhancement is given

by

$$B_{Co} = \simeq \frac{\sum_{a,b} \int_{x_f}^{\infty} \langle \sigma_{ab} v \rangle \gamma_a \gamma_b \frac{dx}{x^2}}{\sum_{A,B} \int_{x_f}^{\infty} \langle \sigma_{AB} v \rangle \Gamma_A \Gamma_B \frac{dx}{x^2}},$$

$$\gamma_a = \frac{g_a (1 + \Delta_a)^{3/2} e^{-\Delta_a x}}{\sum_b g_b (1 + \Delta_b)^{3/2} e^{-\Delta_b x}}, \quad \text{MSSM}$$

$$\Gamma_A = \frac{g_A (1 + \Delta_A)^{3/2} e^{-\Delta_A x}}{\sum_A g_A (1 + \Delta_A)^{3/2} e^{-\Delta_A x}}, \quad \text{MSSM} \otimes \text{Hid.}$$

Here  $a$  runs over the channels which coannihilate in the MSSM sector, while  $A$  runs over channels both in the MSSM sector and in the hidden sector (*i.e.*,  $A = 1, \dots, n_v + n_h$ ). In the limit when the Majoranas in the hidden sector are essentially degenerate with the LSP in the visible sector one has for the case of  $n$  hidden sector  $U(1)$ s the result  $B_{Co} = (1 + d_h/d_v)^2$ , where  $d_s = \sum_s g_s$ , for  $s = (v, h)$ , *i.e.*

$$(\Omega h^2)_{\chi^0} \simeq (1 + \frac{d_h}{d_v})^2 (\Omega h^2)_{\text{MSSM}}. \quad (8.4)$$

When coannihilation effects are negligible in the MSSM sector, one finds that

$$B_{Co} = (1 + 2n)^2. \quad (8.5)$$

Thus a large enhancement of the relic density can occur even for a modest value of  $n$ , *i.e.*,  $n = 3$  leads to  $B_{Co} = 49$  in the degenerate limit[22]. The above phenomenon gives rise to viable models which would otherwise be disallowed due to WMAP constraints. The left panel of Fig.(8.3) shows this effect which is more pronounced when the LSP has a non-negligible Higgsino components. The middle panel of Fig.(8.3) shows the fit the PAMELA data for two model classes with hidden sector LSP components (a pure wino and mixed Higgsino-wino LSP) and the right panel Fig.(8.3) shows the effective mass distributions for these models at the LHC with low luminosity sitting high above the background for the specific Higgsino-wino mixed model.

### 8.2.5. Narrow Resonances at the LHC

As discussed above the Stueckelberg extension of SM and of MSSM lead to a narrow  $Z'$  resonance. Indeed the LHC has the capability to detect resonances of such small widths as the

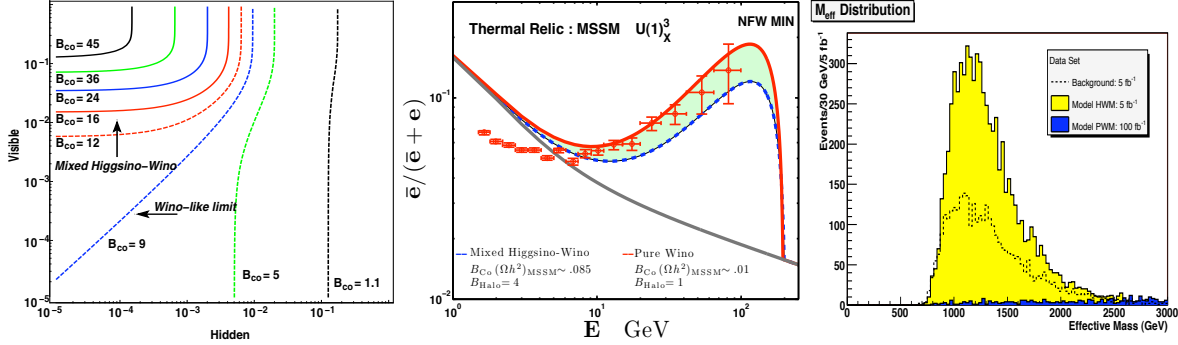


Figure 8.3. Left: Enhancement of the relic density via the presence of spectator states in the HS . Right: Neutralino dark matter producing the PAMELA positron excess for a pure wino and mixed Higgsino-Wino model(HWM) . With three residual  $U(1)_X$  gauge symmetries the Higgsino-wino model can lead to the WMAP relic density. Far Right: A strong LHC signal manifests for the HWM, while the pure wino model has a suppressed LHC signal. From Ref. ([22]) [similar fits as in the middle panel in both the shape and normalizations can be seen in [54]].

di-lepton production can produce a significant number of events above the SM backgrounds[3]. The analysis of Fig.(8.4) shows that even with  $5 \text{ fb}^{-1}$  of integrated luminosity one will be able to discriminate a narrow Stueckleberg  $Z'$  resonance from the standard model background. The leading order cross section (before trigger level cuts) for the model given in Fig.(8.4) reported by Pythia is  $\sigma(pp \rightarrow Z' \rightarrow e^+e^-) = (0.45\text{pb})(0.13)$  for  $(M_1/\text{GeV}, \epsilon) = (500, 0.06)$ . NLO enhancements are expected to introduce an enhancement by a factor of 1.3 – 1.5. The result is in excellent accord with predictions given in [3,4] where previous analyses of the di-lepton cross sections over large mass ranges are given along with general expressions and numerical results for the vector and axial vector couplings of the  $Z'$  with SM fermions.

### 8.2.6. Summary: Stueckelberg Extensions

The Stueckelberg extensions of the SM and of the MSSM give rise to testable signatures of new physics. The minimal model produces a narrow vector resonance that is detectable in the di-lepton channel at the Tevatron and at the LHC [3,4]. At a linear collider the forward-backward asymmetry near the  $Z'$  pole can also provide a detectable signal [2]. Further, if the  $Z'$  decays dominantly into the hidden sector, the mono-jet

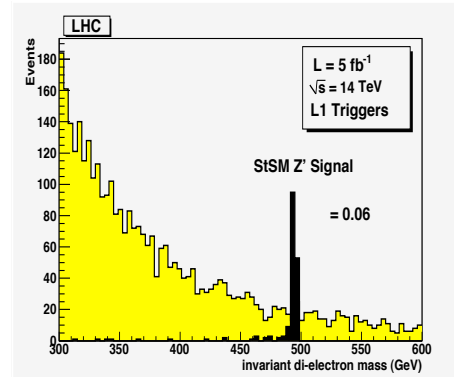


Figure 8.4. Narrow Stueckelberg  $Z'$  at the LHC standing well above the SM backgrounds; the analysis uses PGS4 with L1 triggers only. The Drell-Yan Cross section from Pythia agree with the studies of [3].

signatures can also provide a discovery mode [23]. The supersymmetric extension also predicts the presence of a sharp scalar resonance in the Higgs sector (see [2]).

The predictions in the fermionic sector are also rich with implications for dark matter and for the LHC. The extensions gives rise to three classes of dark matter (a) milli-weak (b) milli-charged

(c) neutralino-like with extra hidden sector degrees of freedom. Thus, the models provide a dirac dark matter candidate [23,4] that can fit the WMAP data when integrating over the Breit-Wigner Poles [4] and can also fit the PAMELA data due the Breit-Wigner enhancement [32] from the  $Z'$  pole. The extensions also lead to a fit on the WMAP and PAMELA data for an LSP with a significant wino component with suppressed hidden sector components[22]. Quite generally the presence of extra weakly interacting hidden sector states provide a boost to the relic density of dark matter due to the presence of extra degrees of freedom in the hidden sector [26,22]. These models can also yield large LHC signatures of supersymmetric event rates for a mixed Higgsino-wino LSP in a significant part of the parameter space. For further related reviews of the Stueckelberg extensions we refer the reader to [56,57,6,58,59,60].

### 8.3. Hidden Valleys

We review a few hidden sector dark matter models, from those that arise in Hidden Valley models, to solutions to the baryon dark matter coincidence.

#### 8.3.1. Overview and basic framework

Over the past several decades a dominant paradigm for dark matter has emerged at the weak scale. In theories that stabilize the Higgs mass at the weak scale, there are often new symmetries that give rise to stable particles. Computing the thermal relic abundance of the weak scale mass particles gives rise, in many of these models, to a dark matter density in accord with what is observed. This remarkable coincidence has been termed the “WIMP miracle,” and is perhaps the most compelling reason to focus theoretically and experimentally on dark matter at the weak scale.

It has been realized in recent years, however, that extensions to the Standard Model can be weakly interacting with the Standard Model while the masses of such states are much lighter than the weak scale, and that in these models the phenomenology can be quite distinct and difficult to uncover at the LHC. This was the focus of the Hidden Valley models [5,6], where a light

gauged hidden sector communicates the the Standard Model through weak scale states, as illustrated in Fig. (1). These models also bear similarities and connection to “quirk” models [61] and unparticles [20].

In these models, states at the TeV scale are often unstable to decay to lighter particles in the hidden sector. This includes, for example, weak scale supersymmetric states that were previously dark matter candidates. Often the lightest  $R$ -odd state will reside in the hidden sector, and the MSSM dark matter candidate will decay to such a light state, modifying the dark matter dynamics and the freeze-out calculation [7].

Is the WIMP miracle thus destroyed in the context of these low mass hidden sectors? In many cases no. This can be for one of two reasons. First, the same annihilation rate for thermal freeze-out can be naturally maintained in these hidden sectors. The annihilation cross-section needed to obtain the observed relic abundance is  $\langle\sigma_{weak}v\rangle \simeq 3 \times 10^{-26} \text{ cm}^3/\text{s}$ , logarithmically sensitive to the dark matter mass. This relation is particularly naturally obtained for weak scale dark matter, since  $g^4/m_X^2 \simeq 3 \times 10^{-26} \text{ cm}^3/\text{s}$  for an  $\mathcal{O}(1)$  gauge coupling  $g$  and weak scale dark matter mass  $m_X$ . However, if  $g \ll 1$  and  $m_X \sim g^2 m_{weak}$ , the relation still holds for much lighter dark matter masses. This is particularly well motivated in the context of gauge mediation, where the dark hidden sector mass scale,  $m_{DHS}$ , is set via two loop graphs,  $m_{DHS}^2 \simeq g^4 F^2 / (M^2 16\pi^2)^2 \log(m_{weak}/m_{DHS})$ . Since  $m_{DHS}$  scales with  $g^2$ , the WIMP miracle still holds for dark matter masses well below the TeV scale, a “WIMPlless miracle”[62]. For  $10^{-2} \lesssim g \lesssim 0.1$ , dark matter in the 0.1 GeV-1 TeV range is naturally obtained. On the other hand, if kinetic mixing is involved, even lower mass scales, such as an MeV, may naturally be induced [12] (though there are strong experimental constraints on such MeV gauged hidden sectors [44]). (For hidden sectors communicating to the Standard Model through kinetic mixing where supersymmetry breaking does not set the mass scale in the hidden sector, see [4,13]. These models are discussed in the previous section.) Depending on whether supersymmetry is predominantly

communicated to the hidden sector through a  $D$ -term or gauge mediated two loop graphs, the mass scale in the hidden sector is  $\sqrt{\epsilon g g_Y m_{weak}}$  or  $\epsilon g g_Y m_{weak}$ , where  $g_Y$  is the hypercharge gauge coupling. For  $\epsilon \simeq 10^{-2} - 10^{-4}$  GeV dark forces are obtained as studied recently in [14,15,42]. For smaller  $\epsilon$ , lower mass dark forces may be obtained. We describe some of these models in more detail in the next section.

The second case where the observed relic abundance is naturally obtained with dark matter mass well below the weak scale is via solutions to the baryon-dark matter coincidence problem. In these cases a light hidden sector is, in many cases, *required* to reproduce the observed relic abundance. The baryon-dark matter coincidence is the fact that observationally  $\Omega_{DM}/\Omega_b \simeq 5$ , while for the standard thermal freeze-out and baryogenesis models, these two quantities are set by unrelated parameters in the model (as in the MSSM, for example, where the dark matter and baryon asymmetries are set largely by dark matter mass and CP asymmetries, respectively).

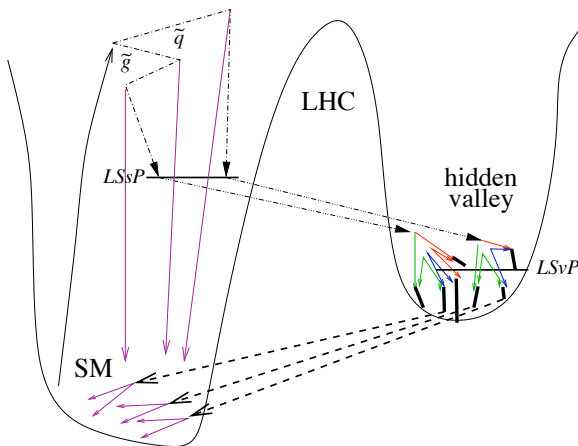


Figure 8.5. A schematic of the Hidden Valley type dark sectors under consideration. From Ref. [7]

Solutions to this problem often relate the asymmetric number densities of the dark matter,  $n_X -$

$n_{\bar{X}}$ , to the baryons (or leptons),  $n_X - n_{\bar{X}} \sim n_b - n_{\bar{b}}$ , where the exact relations are  $\mathcal{O}(1)$  and depend on the particular operator transferring the asymmetries. This relation in turn implies a connection between the baryon (proton) mass and the dark matter mass:  $m_X \sim 5m_p$ , where again the precise factor will depend on the particular operator transferring the asymmetry. In this case the dark matter is low mass and weakly coupled to the Standard Model, residing in a Hidden Valley.

In the remainder of this section, we describe an illustrative model of each type, the kinetic mixing type and the baryon-dark matter coincidence type. We also describe the effects of strong dynamics in particular on the latter type, and lastly turn to discussing collider implications. This discussion is not meant to be in any sense a complete description of these models, but rather a broad overview of the types of hidden sectors that have been constructed. We refer the reader to the appropriate references for details on their construction.

## 8.4. Models of hidden dark matter

### 8.4.1. Low mass dark sectors mediated by kinetic mixing

As we indicated above, low mass dark forces may be particularly well motivated in the context of gauge mediation with kinetic mixing of a new  $U(1)_x$  with hypercharge, as considered in [12,14,15,42]. What happens to the dark force in the hidden sector? As we show here, SUSY breaking effects will induce a vev for the dark Higgses, breaking the dark force and giving it a mass set by the size of the SUSY breaking mass scale in the hidden sector, typically much lower than the TeV scale.

Hypercharge  $D$ -terms will induce a vev for a dark Higgs,  $\phi_i$  in the hidden sector through the potential

$$V_D = \frac{g_x^2}{2} \left( \sum_i x_i |\phi_i|^2 - \frac{\epsilon}{g_x} \xi_Y \right)^2, \quad (8.6)$$

where  $x_i$  is the  $U(1)_x$  charge of the Higgs,  $g_x$  the gauge coupling and  $\xi_Y = -\frac{g_Y}{2} c_{2\beta} v^2$  is the hy-

percharge  $D$ -term, with  $v = 246$  GeV and  $\beta$  the mixing between up and down-type Higgses. This potential induces a vev for the dark Higgs

$$\langle \phi_i \rangle \simeq \left( \frac{\epsilon \xi_Y}{g_x x_i} \right)^{1/2}. \quad (8.7)$$

For  $\epsilon \sim 10^{-3} - 10^{-4}$  the dark  $U(1)_x$  gauge boson acquires a GeV scale mass. For smaller kinetic mixings, smaller gauge boson masses are obtained, even into the MeV range.

There is a subdominant effect, termed Little Gauge Mediation [31,42], which communicates a soft mass to the hidden Higgs of size  $m_{soft}^{hid} \sim \epsilon m_{soft}^{vis}$  through the usual two loop gauge mediation diagrams. More precisely this gives rise to a dark Higgs mass

$$m_{\phi_i}^2 = \epsilon^2 x_I^2 \left( \frac{g_x}{g_Y} \right)^2 m_{Ec}^2, \quad (8.8)$$

where  $m_{Ec}$  is the SUSY breaking mass of the right-handed selectron. These terms are almost always important for determining the precise spectrum of the hidden sectors, particularly when the hypercharge  $D$ -term is zero.

The spectrum in the hidden sector will depend on the precise matter content, however taking a simple anomaly free dark sector

$$W_d = \lambda S \phi \bar{\phi}, \quad (8.9)$$

results in one stable,  $R$ -odd fermion, whose mass is either  $\lambda \langle \phi \rangle$  or  $\sqrt{2} x_H g_x \langle \phi \rangle$ .

In these models the dark matter mass is set by thermal freeze-out, and for some ranges of parameters and mass spectra a ‘‘WIMPless miracle’’ for dark matter in the MeV to tens of GeV mass range naturally results [42]. While in some classes of these low mass hidden sector models, thermal freeze-out naturally results in the right relic abundance, we now turn to a class of models where GeV mass states will automatically give the correct relic abundance: solutions to the baryon-dark matter coincidence.

#### 8.4.2. Low mass dark sectors as solutions to the baryon-dark matter coincidence

There are a number of solutions to the baryon-dark matter coincidence in the literature

[63], especially in the context of technicolor [64]. We focus here on a particularly simple class which fits the paradigm of the low mass hidden sector, or Hidden Valley. This particular class of models is termed Asymmetric Dark Matter [65], and in these cases the dark matter candidate is not derived from models designed to stabilize the weak scale.

The idea behind these models is to write an effective field theory which describes the interactions between the hidden sector and visible sector (integrating out the fields residing at the ‘‘pass’’ in Fig. (1), which transfers a Standard Model baryon or lepton asymmetry to the dark sector. The dark matter in these models must be sterile, so this limits the number of operators which can be constructed to accomplish this purpose. In particular, in the context of supersymmetry, the lowest dimension operators carrying lepton or baryon number which are sterile are  $udd$  and  $LH$ . If these operators are connected to the hidden sector containing the dark field  $\bar{X}$  to transfer an asymmetry, we have

$$W = \frac{\bar{X}^2 udd}{M^2} \quad (8.10)$$

$$W = \frac{\bar{X}^2 LH}{M}.$$

The second operator, for example, enforces  $2(n_X - n_{\bar{X}}) = n_{\bar{\ell}} - n_{\ell}$ , and a detailed calculation relating the lepton asymmetry to the baryon asymmetry (through sphalerons) consequently shows that this model predicts  $m_X \simeq 8$  GeV. Note that we added  $\bar{X}^2$  and not  $X$ , since the additional  $Z_2$  symmetry ensures DM stability. In some other cases [66],  $R$ -parity may be utilized instead to stabilize the dark matter

Now once the Standard Model baryon or lepton asymmetry has been transferred to the dark sector, the symmetric part of the dark matter (which is much larger than the asymmetric part,  $n_X + n_{\bar{X}} \gg n_X - n_{\bar{X}}$ ) must annihilate, leaving only the asymmetric part. There are a variety of mechanisms to do this, but the difficulty here is having a mechanism which is efficient enough annihilate away the whole of the symmetric part through  $X\bar{X} \rightarrow SM$ . Such a process, through a

dimension six operator has a cross-section

$$\sigma v = \frac{1}{16\pi} \frac{m_X^2}{M'^4}. \quad (8.11)$$

This cross-section must be bigger than approximately 1 pb in order to reduce the dark matter density to its asymmetric component, implying  $M' \lesssim 100$  GeV, a rather severe constraint for any new electroweak state coupling to Standard Model states.

Here confinement in the hidden sector can be a useful tool. If the dark matter consists of symmetric and asymmetric bound states of elementary dark sector fermions, the symmetric states may decay through the same dimension six operators, while the asymmetric states would remain stable. For example, suppose in the operator Eq. (8.10), we replaced the operator  $\bar{X}^2$  with  $\bar{v}_1 v_2$ , and supposing these  $v_1$  and  $v_2$  constituents are charged under a hidden sector confining gauge group, such that bound states  $\bar{v}_1 v_2$ ,  $\bar{v}_2 v_1$  and  $\bar{v}_1 v_1 + \bar{v}_2 v_2$  are the relevant degrees of freedom at low energies. When Eq. (8.10) freezes out, the asymmetric  $\bar{v}_1 v_2$  states remain stable, while the symmetric  $\bar{v}_1 v_1 + \bar{v}_2 v_2$  states decay rapidly through less suppressed operators (that is, we take  $M' \ll M$ ). In the next section we describe a related class of confinement models where the constituents of the dark matter bound states carry electroweak charges. In these models sphalerons rather than higher dimension operators such as Eq. (8.10) to transfer the asymmetry.

#### 8.4.3. Dark sectors with confinement

We now illustrate a dark sector model with confinement recently considered in [67]. We note that these models bear some similarity to models constructed earlier in the context of technicolor [64]. The new defining characteristic of this hidden sector model is the presence of a new non-abelian gauge group which confines *at a low scale*. The dark matter candidate is a *charge neutral* composite of electroweak charged, weak scale mass, “quirks.” These quirks,  $U$  and  $D$  are analogous to quarks except they carry a new global charge that keeps one combination,  $UD$ , stable ( $U$  and  $D$  carry opposite electric charge). That is, analogous to the proton, the dark matter is a composite

dark baryon. In the language of Fig. (1), the low mass dark glueballs resides in the hidden sector, while the dark matter constituents are themselves heavy weak scale fields and act as the connectors between the Standard Model and dark glue sector.

Since the constituents are electroweak charged, they can be processed by sphalerons. In particular, the sphalerons will violate some linear combination of  $B$ ,  $L$  and dark baryon number,  $DB$ . Thus an asymmetry in  $B$  and  $L$  (produced from some leptogenesis or baryogenesis mechanism) will be converted to an asymmetry in  $DB$ . The  $DB$  asymmetry then sets the dark matter relic density. Since the dark matter mass is around the mass of the weak scale quirk constituents, there must be a Boltzmann suppression in  $DB$  to achieve the observed relation  $\Omega_{DM} \simeq 5\Omega_b$ . This can be naturally achieved when the sphalerons decouple just below the dark matter mass:

$$\Omega_{DM} \sim \frac{m_{DM}}{m_p} e^{-m_{DM}/T_{sph}} \Omega_b, \quad (8.12)$$

where  $T_{sph}$  is the sphaleron decoupling temperature, and the exact proportions are worked out in [67].

These dark sectors with confinement have also effectively been used to achieve the mass splittings necessary to realize the inelastic [68,69] and exciting [70] dark matter scenarios [40]. In these models the dark matter is again a weak scale composite with the confinement scale of the gauge group binding the constituents at the 100 keV-MeV. The result is mass splittings between the dark matter ground state and excited states set by the confinement scale, and these mass splittings are phenomenologically of the size to fit DAMA [71] and INTEGRAL [72] observations through the excitation of the dark matter ground state to one of the higher states, which then decays back to the ground state, producing  $e^+e^-$  or resulting in an inelastic scattering of dark matter off nuclei.

#### 8.4.4. Collider signatures

The collider signatures for these models can be as diverse as the dark sectors themselves. These include displaced vertices from hidden sector de-

cays, dark hadronization jets and lepton jets. We draw attention here to some of the collider signatures which are not discussed elsewhere in this paper.

First, as pointed out in [7], the presence of Hidden Valleys with supersymmetry causes the MSSM lightest supersymmetric partner to decay to hidden sector states. For example, through the operators Eq. (8.10), the neutralino can have exotic decays to light dark matter states, such as  $\chi^0 \rightarrow \nu \tilde{X} \tilde{X}$ ,  $h^- \ell^+ \tilde{X} \tilde{X}$  or  $\chi^0 \rightarrow XXqqq$ . The phenomenology of these models remains to be studied further.

In other models discussed here, once the dark states are produced, cascade decays in the hidden sector are completely invisible, and as a result the only signature is missing energy. In this case, how does one ascertain the nature of the dark sector and extract key information? Information about the hidden sector must be obtained in this case utilizing initial state radiation (ISR), as a jet or photon radiated off an initial state quark or lepton [4,23,24]. An example is the invisible  $Z'$ : in these models a  $Z'$  couples to both the hidden and visible sectors, so that the  $Z'$  has a significant hidden decay branching fraction. One way to search for these models is to simply do a counting experiment [24]: look for an excess of mono-photon or mono-jet plus missing energy. As shown in Fig. (2), for a  $Z'$  mass below  $\sim 1$  TeV, even such a simple counting experiment can uncover new physics. The signal required to discover an invisibly decaying  $Z'$  with initial state photon for 10, 30 and 100  $\text{fb}^{-1}$  is compared against typical invisible decay signals for sequential and  $U(1)_\chi$   $Z'$ 's. Further signal separation could be achieved using more sophisticated event shape variables.

#### 8.4.5. Summary of Low Mass Dark Sectors

As we have discussed, there are broad classes of models of low mass hidden dark matter that retain many of the phenomenological successes of weak scale, weakly interacting particles. We have outlined three such classes, the first where the light dark sector communicates to the Standard Model through light states which have, however, small interactions with Standard Model states through kinetic mixing (or simply small gauge couplings). Though the dark matter is much

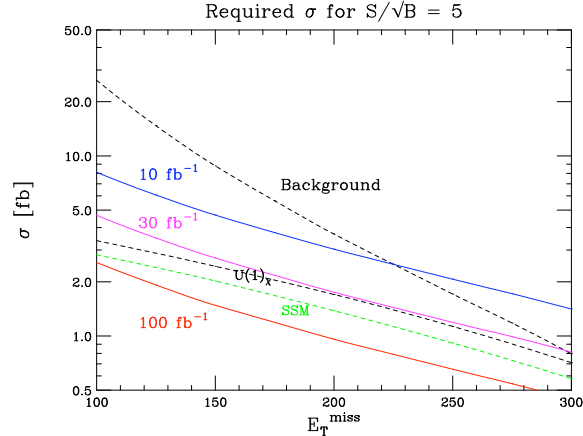


Figure 8.6. Required cross-section to discover at  $5\sigma$  an invisibly decaying  $Z'$  with mono-photon plus missing energy for 10, 30 and 100  $\text{fb}^{-1}$ , along with the expected signals from two invisibly decaying  $Z'$ , from the sequential standard model and  $U(1)_\chi$ . From Ref. [24].

lighter than the weak scale, in some of these models the WIMP miracle is still obtained, and the observed relic density of dark matter is produced. Second, we looked at Asymmetric Dark Matter models, where a dark matter mass near the proton mass is necessary to give rise to the observed relic abundance. Third, we examined cases where these dark sectors feature new confining gauge groups with a low confinement scale as in a Hidden Valley, quirk or unparticle model.

In summary, we are beginning to learn that the dark sector could be complex – it may not be simply a single, stable, weakly interacting particle. There may be multiple resonances in the hidden sector with an array of new forces that govern their interactions, from confining gauge groups to a dark  $U(1)$ . And this new dynamics need not reside at the weak scale, opening new avenues for exploration.

### 8.5. Probing the GeV dark sector at the LHC

Dark matter can carry  $\text{GeV}^{-1}$  scale self-interactions. The GeV force carrier and associated states constitute a so-called dark sector. We outline the LHC signals of such a dark sector.

#### 8.5.1. Overview

Motivated by astrophysical observations, it has been proposed [14] (see also [13]) that electroweak scale dark matter ( $m_{\text{DM}} \sim \text{TeV}$ ) have  $\text{GeV}^{-1}$  range self-interactions. The force carrier and associated states are collectively referred to as “the dark sector”. In order to account for the excesses in the cosmic ray observations, the dark sector generically also couples the Standard Model states. To satisfy the experimental constraints, such couplings (the “portal”), are expected to be tiny. More specific model buildings for the dark sector have been carried out in [31,47,15,37,17,38,42,43,46,40,33]. We also note that this class of models can be regarded as a distinct possibility of the hidden valley scenario [5,6].

#### 8.5.2. Basic framework

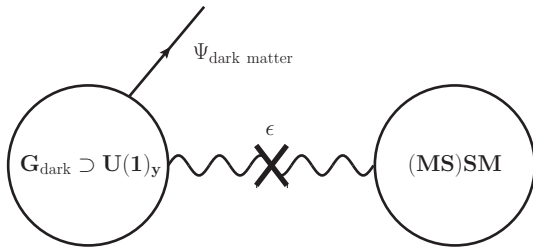


Figure 8.7. A schematic of the setup under consideration. Dark matter carries  $\text{GeV}^{-1}$  range self-interaction  $G_{\text{dark}}$ . The GeV dark sector couples to the SM via some small coupling  $\epsilon$ .

A schematic setup for the dark sector model is shown in Fig. 8.7. Different choices of  $G_{\text{d}}$  and the portal to the Standard Model have been considered [33]. In the following, we will focus on the

case in which  $G_{\text{d}}$  is a gauge interaction, and the portal is generated by kinetic mixing between an  $U(1)_y$  factor of  $G_{\text{d}}$  and the hypercharge  $U(1)_Y$ . In the following, we will discuss the most relevant part of the Lagrangian from which the most generic signals can be derived. The kinetic mixing can be parameterized as [16]

$$\begin{aligned} \mathcal{L}_{\text{gauge mix}} &= -\frac{1}{2}\epsilon_1 b_{\mu\nu} A^{\mu\nu} - \frac{1}{2}\epsilon_2 b_{\mu\nu} Z^{\mu\nu} \\ &= -\frac{1}{2}\epsilon'_1 b_{\mu\nu} B^{\mu\nu} - \frac{1}{2}\epsilon'_2 b_{\mu\nu} W_3^{\mu\nu} \end{aligned} \quad (8.13)$$

where  $b_{\mu\nu}$  denotes the field strength for the dark gauge boson and  $\epsilon_{1,2}$  and  $\epsilon'_{1,2}$  are related by the Weinberg angle. In particular, when only  $\epsilon'_1$  is present, we have  $\epsilon_1 = \epsilon'_1 \cos \theta_W$  and  $\epsilon_2 = \epsilon'_1 \sin \theta_W$ <sup>1</sup>. In supersymmetric scenarios, there is also an identical mixing between the gauginos

$$\mathcal{L}_{\text{gaugino mix}} = -2i\epsilon'_1 \tilde{b}^\dagger \bar{\sigma}^\mu \partial_\mu \tilde{B} - 2i\epsilon'_2 \tilde{b}^\dagger \bar{\sigma}^\mu \partial_\mu \tilde{W}_3 \quad (8.14)$$

The kinetic mixings can be removed from by appropriate field redefinitions, which lead to the portal couplings

$$\begin{aligned} \mathcal{L}_{\text{portal}} &= \epsilon_1 b_\mu J_{\text{EM}}^\mu + \epsilon_2 Z_\mu J_b^\mu \\ &+ \epsilon'_1 \tilde{B} \tilde{J}_b + \epsilon'_2 \tilde{W}_3 \tilde{J}_b, \end{aligned} \quad (8.15)$$

$$J_b^\mu = g_d \sum_i q_i \left( i(h_i^\dagger \partial^\mu h_i - h_i \partial^\mu h_i^\dagger) + \tilde{h}_i^\dagger \bar{\sigma}^\mu \tilde{h}_i \right)$$

$$\tilde{J}_b = -i\sqrt{2}g_d \sum_i q_i \tilde{h}_i^\dagger h_i \quad (8.16)$$

where  $J_{\text{EM}}$  is the SM electromagnetic current.  $J_b$  contains dark scalar and dark fermion bilinears, and  $\tilde{J}_b$  contains mixed dark scalar-fermion bilinears. We will consider couplings in the range  $\epsilon_i \sim 10^{-3} - 10^{-4}$ , which satisfies all the constraints (For recent studies, see [35,41] and references therein.) and can arise naturally in models.

We will focus on the simplest case  $G_{\text{d}} = U(1)_y$  (and denote  $b_\mu$  as dark photon) for the rest of note, which encapsulates the main features of dark sector phenomenology [15,16,17]. We will highlight the new features from a more complicated dark sector.

<sup>1</sup>  $\epsilon'_2$  can arise from higher dimensional operators such as  $b_{\mu\nu} \text{tr}(H^\dagger W^{\mu\nu} H)/\Lambda^2$ . We will not focus on this situation here, as it will not qualitatively change the phenomenology.

### 8.5.3. Production at the LHC

We will discuss in this section relevant production channels for the LHC search for the GeV dark sector. The relevant rates are shown in Fig. 8.8. Such GeV dark sector states will decay back to Standard Model light states, such as leptons, and produce distinct signals which we will discuss in detail in the next section.

**Prompt “dark photon”.** We see from the first term in Eq. 8.15 that the dark  $U(1)_y$  couples just like the Standard Model photon, except with a coupling suppressed by  $e_{\text{eff}}/e \equiv \epsilon_1$ . Therefore, the dark photon,  $\gamma' \equiv b_\mu$ , should be produced just like the Standard Model photon (with a much smaller rate), for example, through the prompt photon process  $pp \rightarrow \gamma' + X$ .

**Rare Z decay.** The second term in Eq. 8.15 implies that the Standard Model  $Z^0$  has a rare decay mode into the dark sector, with a branching ratio proportional to  $\epsilon_2^2$ .

**SUSY electroweak-ino production.** Supersymmetry provides natural setups of the GeV dark sector, in which both the GeV scale and small portal coupling are generated in very simple models [15,16,17]. The presence GeV dark sector dramatically changes the SUSY phenomenology [34,15,16]. In particular, LSP will decay into the dark sector through the last two couplings in Eq. 8.15, the subsequent decay of the dark sector states will result in collimated Standard Model charged leptons. As the LSP is always present at the end of any SUSY decay chain, the production rates for dark sector states are just the production rates of the electroweak-inos. Of course, the dark sector states can also be produced in longer SUSY decay chains starting with colored superpartners, with hard jets. Although not as clean as the direct electroweak-ino production, it can certainly be a very useful channel given the larger production rate of the colored superpartners.

**Dark sector cascade and parton shower.** The dark sector typically has at least several states. Heavier dark sector states, after being produced through one of channels mentioned above, will cascade down to lighter states. In addition, if the dark sector gauge coupling is not so small, dark sector state can have “dark radiations” similar to the QCD and QED radiations.

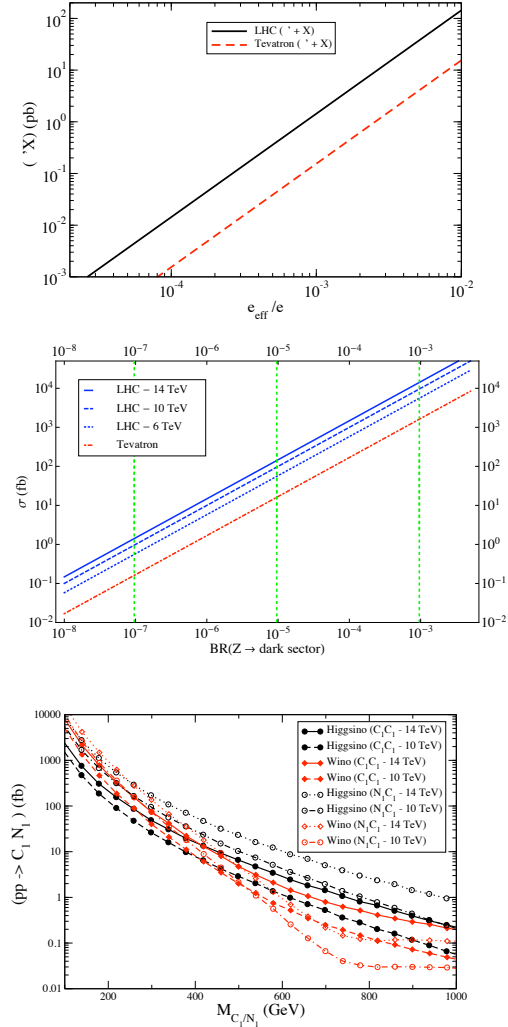


Figure 8.8. Rates of dark sector production processes. Top: prompt dark photon at the LHC ( $E_{\text{cm}} = 14$  TeV); middle: rare Z decay at the LHC,  $\alpha_d = 1/127$ ; bottom: some important SUSY electroweak-ino production processes. See text for detailed explanation.

Signals: lepton jets and beyond:

We begin by describing the decay of the dark sector states back to the Standard Model.

#### Dark photon and lepton jet

The first term in Eq. 8.15 implies that the dark photon will decay into charged particles of the Standard Model. Since  $m_{b_\mu} \sim \text{GeV}$ , typically the dominant channels are  $e^+e^-$ ,  $\mu^+\mu^-$ , and  $\pi^+\pi^-$ ,

with significant branching ratios into the leptonic channels (for recent studies see [35,41],[73]). Since the dark photon are produced at the LHC typically with large boost, for example  $\gamma = m_Z/2m_{b_\mu} \sim 50$  from Z decay, the resulting decay products are highly collimated. This leads to a class of unique objects, *lepton jets* [34,15,16], which are high collimated energetic leptons. The typical multiplicity of the leptons in a lepton jet is model dependent. A dark photon decays into a pair of leptons. Cascade, and parton showering, in the dark sector can lead to higher multiplicities (possibly 4 or more). For the range of  $\epsilon$ s under consideration, the decay of dark photon is almost always prompt.

#### Dark Higgs

The dark gauge interaction must be spontaneously broken at around a GeV, which can be achieved by introducing a dark Higgs sector. The dark Higgs particles can be produced at the LHC through Z and LSP decay, and possibly through a dark sector cascade. Heavier dark Higgses will cascade down to the lighter ones and possibly lighter dark gauge bosons. The LHC signal of the dark higgs sector depends on the mass of the lightest dark higgs in comparison with  $m_{b_\mu}$ . If  $m_{h_d} > 2m_{b_\mu}$ , we have  $h_d \rightarrow b_\mu b_\mu$ , followed by  $b_\mu$  decay, giving rise to multiple ( $> 4$ ) lepton final states which reconstruct 2 dark photon resonances and the dark Higgs. If  $m_{b_\mu} < m_{h_d} < 2m_{b_\mu}$ , we have  $h_d \rightarrow b_\mu^* b_\mu$ . The final state is similar to the previous case with less reconstructed resonances. There is also a possibility of having displaced vertices in this case. If  $m_{h_d} < m_{b_\mu}$ , dark Higgs will decay either to a 4 body final state through 2 off-shell  $b_\mu^*$ , or to 2 body final states through a loop process. In either case, the decay lifetime is much longer than the detector time scale, and the dark higgs will leave its trace as missing energy.

#### More details of the Signal

A more detailed study of lepton jets from electroweak processes, including Z and LSP decay, has been carried out in Ref. [16]. In this more realistic study, an isolation criterion is adopted. We require that: Two or more leptons each with  $p_T > 10$  GeV inside a cone of  $\Delta R < 0.1$  with hadronic/leptonic isolation cut of  $\sum p_T < 3$  GeV

in an annulus of  $0.1 < \Delta R < 0.4$  around the lepton jet. We have included the effect of dark sector parton showering (in the simple case of  $G_d = U(1)$ ). The decay branching ratios of dark photon into leptonic and pion final states have been properly taken into account. We find that

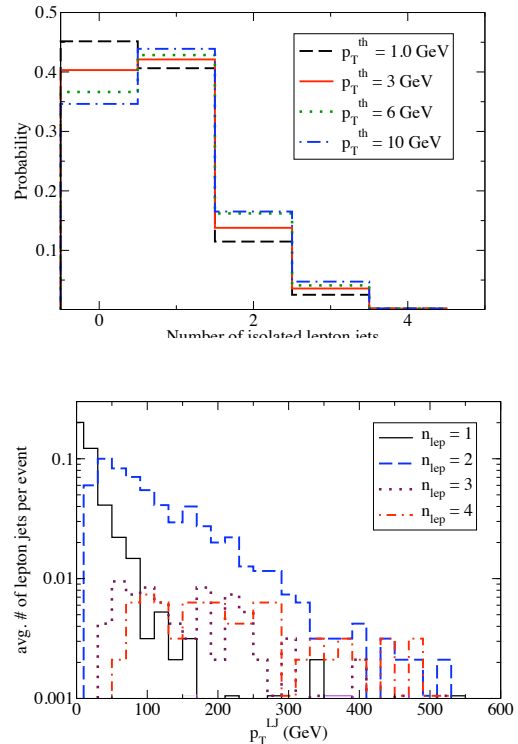


Figure 8.9. Top: lepton jet efficiency; bottom: lepton multiplicity and lepton jet  $p_T$ .  $m_{\text{LSP}} = 300$  GeV,  $\alpha_d = 0.1$ .

1. The efficiency of having well isolated lepton jet(s) is significant. We see from Fig. 8.9 that for electroweak-ino production, more than half of the event will have at least one well isolated lepton jet.

2. The hardest leptons are dominantly from the decay of the dark photon coming directly from the decay of the LSP (or Z), while the radiated dark photons (in the weakly coupled models) typically contribute a number of soft (several to 10s of GeV) leptons. Lepton jets with 2 leptons receive contributions from both direct decay and

radiation. Lepton jets with 3 or more leptons are dominated by the direct decay, as a result, the leptons are more energetic, see Fig. 8.9.

3. There are indeed a large number of isolated leptons. Typically coming from the decay of soft dark photons, they are less energetic. A significant fraction of them could still be hard enough,  $\geq 10$  GeV, to be useful.

4. The results shown here is for a particular choice of dark gauge coupling and leptonic decay branching ratio. See Ref. [16] for more detailed studies with different choices of parameters. Generically, the effect of radiation decreases (increases) linearly with smaller (larger) dark gauge couplings, from almost no radiation (with small coupling) to the case where there is no clear distinction between direct decay and radiation.

#### 8.5.4. Summary of GeV Dark Sector Signatures

- Lepton jet recoiling against a QCD-jet would be an inclusive search for a prompt dark photon production.
- Two lepton jets recoiling against each other and reconstructing the  $Z^0$  would be an interesting signal of rare  $Z^0$  decays into the dark sector and can be looked for at LEP, Tevatron, and LHC.
- Two (or more) lepton jets together with missing energy and possibly other isolated final states (e.g. a muon, an electron, and etc.) can be the result of electroweak-ino production and their eventual cascade into the dark sector.
- Lepton jets in association with QCD-jets could be the result of strong production of colored particles which eventually cascade into the dark sector.

## 8.6. Conclusions

The analyses presented here show that in a variety of settings the presence of a hidden sector gives rise to unique signatures in both collider physics and in the hunt for dark matter. The mechanisms for communication between the hidden and visible sectors, aside from by gravity, could be via  $U(1)$  gauge fields in the hidden sector which mix with the gauge fields in the visible sector via kinetic mixings or via mass mixing by

the Stueckelberg mixing mechanism, or via higher dimensional operators.

Specifically, in Sec.(8.2) hidden sector extensions with Stueckelberg mass and kinetic mixing were discussed which lead to several new models of dark matter and a host of new physics signatures both in dark matter experiments and at the LHC; the most striking of which at hadron colliders would be a very narrow  $Z$  prime resonance in the di-lepton channel accompanied by an excess of positrons from the galactic halo due to a Breit-Wigner pole enhancement. These phenomena would help pinpoint the mass of the dark matter particle. In Sec.(8.3) classes of hidden sector models with low mass dark matter were reviewed which can arise via kinetic mixings, as well as via asymmetric dark matter models, and dark sectors with a new confining gauge groups which are natural in a Hidden Valley, a quirk or unparticle model. Collider implications of a invisibly decaying  $Z$  prime was also re-emphasized. In Sec.(8.5) photon, lepton and jet signatures of dark sectors with a GeV mass  $Z'$  particle were reviewed in both supersymmetric and non-supersymmetric models with kinetic mixings. Discovery prospects at the LHC in several channels were discussed in detail.

In summary, the models discussed here provide visible signatures of hidden symmetries. With the turn on of the LHC and forthcoming data from several dark matter experiments, the hidden sector models of the type discussed above can be put to the test on both fronts.

## REFERENCES

1. B. Kors and P. Nath, Phys. Lett. B **586**, 366 (2004); [arXiv:hep-ph/0402047]; JHEP **0412**, 005 (2004) [arXiv:hep-ph/0406167].
2. B. Kors and P. Nath, JHEP **0507**, 069 (2005). [arXiv:hep-ph/0503208].
3. D. Feldman, Z. Liu and P. Nath, Phys. Rev. Lett. **97**, 021801 (2006), [arXiv:hep-ph/0603039]; JHEP **0611**, 007 (2006), [arXiv:hep-ph/0606294].
4. D. Feldman, Z. Liu and P. Nath, Phys. Rev. D **75**, 115001 (2007), [arXiv:hep-ph/0702123].
5. M. J. Strassler and K. M. Zurek, Phys. Lett.

- B **651**, 374 (2007), [arXiv:hep-ph/0604261];
6. M. J. Strassler and K. M. Zurek, Phys. Lett. B **661**, 263 (2008), [arXiv:hep-ph/0605193].
  7. M. J. Strassler, arXiv:hep-ph/0607160.
  8. T. Han, Z. Si, K. M. Zurek and M. J. Strassler, JHEP **0807**, 008 (2008), [arXiv:0712.2041 [hep-ph]].
  9. B. Holdom, Phys. Lett. B **166**, 196 (1986); H. Goldberg and L. J. Hall, Phys. Lett. B **174**, 151 (1986); B. Holdom, Phys. Lett. B **259**, 329 (1991); R. Foot, H. Lew and R. R. Volkas, Phys. Lett. B **272**, 67 (1991).
  10. K. R. Dienes, C. F. Kolda and J. March-Russell, Nucl. Phys. B **492**, 104 (1997); S. A. Abel and B. W. Schofield, Nucl. Phys. B **685**, 150 (2004).
  11. J. Kumar and J. D. Wells, Phys. Rev. D **74**, 115017 (2006); W. F. Chang, J. N. Ng and J. M. S. Wu, Phys. Rev. D **74**, 095005 (2006); J. D. Wells, arXiv:0909.4541 [hep-ph].
  12. D. Hooper and K. M. Zurek, Phys. Rev. D **77**, 087302 (2008).
  13. M. Pospelov, A. Ritz and M. B. Voloshin, Phys. Lett. B **662**, 53 (2008); M. Pospelov, A. Ritz Phys. Lett. B **671**, 391 (2009).
  14. N. Arkani-Hamed, D. P. Finkbeiner, T. R. Slatyer and N. Weiner, Phys. Rev. D **79**, 015014 (2009), [arXiv:0810.0713 [hep-ph]].
  15. M. Baumgart, C. Cheung, J. T. Ruderman, L. T. Wang and I. Yavin, JHEP **0904**, 014 (2009), [arXiv:0901.0283 [hep-ph]].
  16. C. Cheung, J. T. Ruderman, L. T. Wang and I. Yavin, arXiv:0909.0290 [hep-ph].
  17. C. Cheung, J. T. Ruderman, L. T. Wang and I. Yavin, Phys. Rev. D **80**, 035008 (2009), [arXiv:0902.3246 [hep-ph]].
  18. S. A. Abel, M. D. Goodsell, J. Jaeckel, V. V. Khoze and A. Ringwald, JHEP **0807**, 124 (2008); M. Ahlers, J. Jaeckel, J. Redondo and A. Ringwald, Phys. Rev. D **78**, 075005 (2008).
  19. C. P. Burgess, J. P. Conlon, L. Y. Hung, C. H. Kom, A. Maharana and F. Quevedo, JHEP **0807**, 073 (2008).
  20. H. Georgi, Phys. Rev. Lett. **98**, 221601 (2007); J. J. van der Bij and S. Dilcher, Phys. Lett. B **655**, 183 (2007); K. Cheung, W. Y. Keung and T. C. Yuan, Phys. Rev. Lett. **99**, 051803 (2007); M. J. Strassler, arXiv:0801.0629 [hep-ph].
  21. H. Goldberg and P. Nath, Phys. Rev. Lett. **100**, 031803 (2008).
  22. D. Feldman, Z. Liu, P. Nath and B. D. Nelson, arXiv:0907.5392 [hep-ph]; To appear in PRD;
  23. K. Cheung and T. C. Yuan, JHEP **0703**, 120 (2007). [arXiv:hep-ph/0701107].
  24. F. J. Petriello, S. Quackenbush and K. M. Zurek, Phys. Rev. D **77**, 115020 (2008); Y. Gershtein, F. Petriello, S. Quackenbush and K. M. Zurek, Phys. Rev. D **78**, 095002 (2008).
  25. E. Dudas, Y. Mambrini, S. Pokorski and A. Romagnoni, arXiv:0904.1745 [hep-ph].
  26. D. Feldman, B. Kors and P. Nath, Phys. Rev. D **75**, 023503 (2007), [arXiv:hep-ph/0610133].
  27. J. Kumar, A. Rajaraman and J. D. Wells, Phys. Rev. D **77**, 066011 (2008).
  28. J. H. Huh, J. E. Kim, J. C. Park and S. C. Park, Phys. Rev. D **77**, 123503 (2008).
  29. R. Lu and Q. Wang, Chin. Phys. Lett. **24**, 3371 (2007).
  30. A. Ibarra, A. Ringwald and C. Weniger, JCAP **0901**, 003 (2009).
  31. K. M. Zurek, Phys. Rev. D **79**, 115002 (2009).
  32. D. Feldman, Z. Liu, P. Nath Phys. Rev. D **79**, 063509 (2009).
  33. Y. Nomura and J. Thaler, Phys. Rev. D **79**, 075008 (2009).
  34. N. Arkani-Hamed and N. Weiner, JHEP **0812**, 104 (2008).
  35. M. Pospelov, arXiv:0811.1030 [hep-ph]
  36. S. Baek and P. Ko, arXiv:0811.1646 [hep-ph].
  37. E. J. Chun and J. C. Park, arXiv:0812.0308 [hep-ph].
  38. A. Katz and R. Sundrum, JHEP **0906**, 003 (2009).
  39. S. Cassel, D. M. Ghilencea and G. G. Ross, arXiv:0903.1118 [hep-ph].
  40. D. S. M. Alves, S. R. Behbahani, P. Schuster and J. G. Wacker, arXiv:0903.3945 [hep-ph].
  41. M. Reece and L. T. Wang, JHEP **0907**, 051 (2009).
  42. D. E. Morrissey, D. Poland and K. M. Zurek, JHEP **0907**, 050 (2009).

43. J. L. Feng, M. Kaplinghat, H. Tu and H. B. Yu, *JCAP* **0907**, 004 (2009).
44. J. D. Bjorken, R. Essig, P. Schuster and N. Toro, arXiv:0906.0580 [hep-ph].
45. Y. Mambrini, arXiv:0907.2918 [hep-ph].
46. M. Goodsell, J. Jaeckel, J. Redondo and A. Ringwald, arXiv:0909.0515 [hep-ph].
47. F. Chen, J. M. Cline and A. R. Frey, arXiv:0907.4746 [hep-ph].
48. A. Dedes, I. Giomataris, K. Suxho and J. D. Vergados, arXiv:0907.0758 [hep-ph].
49. O. Adriani *et al.* [PAMELA Collaboration], *Nature* **458**, 607 (2009); *Phys. Rev. Lett.* **102**, 051101 (2009).
50. A. Abulencia *et al.* [CDF Collaboration], *Phys. Rev. Lett.* **95**, 252001 (2005); *Phys. Rev. Lett.* **96**, 211801 (2006); V. M. Abazov *et al.* [D0 Collaboration], *Phys. Rev. Lett.* **95**, 091801 (2005); *Phys. Lett. B* **641**, 415 (2006); O. Stelzer-Chilton [CDF Collaboration and D0 Collaboration], arXiv:0810.4754 [hep-ex]; T. Aaltonen *et al.* [CDF Collaboration], *Phys. Rev. Lett.* **102**, 031801 (2009); [arXiv:0810.2059 [hep-ex]]; arXiv:0811.0053 [hep-ex]; K. Hatakeyama [CDF Collaboration], arXiv:0810.3681 [hep-ex].
51. P. Langacker, arXiv:0801.1345 [hep-ph].
52. C. Coriano, N. Irges and E. Kiritsis, *Nucl. Phys. B* **746**, 77 (2006); R. Armillis, C. Coriano and M. Guzzi, *JHEP* **0805**, 015 (2008) [arXiv:0711.3424 [hep-ph]].
53. P. Anastasopoulos, F. Fucito, A. Lionetto, G. Pradisi, A. Racioppi and Y. S. Stanev, *Phys. Rev. D* **78** (2008) 085014 [arXiv:0804.1156 [hep-th]].
54. P. Grajek, G. Kane, D. Phalen, A. Pierce and S. Watson, arXiv:0812.4555; G. Kane, R. Lu and S. Watson, arXiv:0906.4765 [astro-ph.HE]; J. Hisano, M. Kawasaki, K. Kohri and K. Nakayama, *Phys. Rev. D* **79**, 063514 (2009).
55. D. Feldman, Z. Liu, P. Nath and B. D. Nelson, arXiv:0907.5392 [hep-ph]; To appear in PRD; A. Arvanitaki, N. Craig, S. Dimopoulos, S. Dubovsky and J. March-Russell, arXiv:0909.5440 [hep-ph].
56. B. Kors and P. Nath, arXiv:hep-ph/0411406.
57. D. Feldman, Z. Liu and P. Nath, *AIP Conf. Proc.* **939**, 50 (2007).
58. P. Nath, arXiv:0812.0958 [hep-ph].
59. P. Langacker, arXiv:0909.3260 [hep-ph].
60. Z. Liu, arXiv:0910.0061 [hep-ph].
61. J. Kang and M. A. Luty, arXiv:0805.4642 [hep-ph].
62. J. L. Feng and J. Kumar, *Phys. Rev. Lett.* **101**, 231301 (2008).
63. S. Dodelson, B. R. Greene and L. M. Widrow, *Nucl. Phys. B* **372**, 467 (1992). V. Kuzmin, *Phys. Part. Nucl.* **29**, 257 (1998), *Fiz. Elem. Chast. Atom. Yadra* **29**, 637 (1998), *Phys. Atom. Nucl.* **61**, 1107 (1998); M. Fujii and T. Yanagida, *Phys. Lett. B* **542**, 80 (2002); R. Kitano and I. Low, *Phys. Rev. D* **71**, 023510 (2005); R. Kitano, H. Murayama and M. Ratz, *Phys. Lett. B* **669**, 145 (2008); G. R. Farrar and G. Zaharijas, *Phys. Rev. Lett.* **96**, 041302 (2006); D. Hooper, J. March-Russell and S. M. West, *Phys. Lett. B* **605**, 228 (2005); L. Roszkowski and O. Seto, *Phys. Rev. Lett.* **98**, 161304 (2007); O. Seto and M. Yamaguchi, *Phys. Rev. D* **75**, 123506 (2007); M. Aoki, S. Kanemura and O. Seto, *Phys. Rev. D* **80**, 033007 (2009).
64. S. Nussinov, *Phys. Lett. B* **165**, 55 (1985). S. M. Barr, R. S. Chivukula and E. Farhi, *Phys. Lett. B* **241**, 387 (1990). S. B. Gudnason, C. Kouvaris and F. Sannino, *Phys. Rev. D* **73**, 115003 (2006); R. Foadi, M. T. Frandsen and F. Sannino, *Phys. Rev. D* **80**, 037702 (2009).
65. D. E. Kaplan, M. A. Luty and K. M. Zurek, *Phys. Rev. D* **79**, 115016 (2009) [arXiv:0901.4117 [hep-ph]].
66. S. Chang and M. A. Luty, arXiv:0906.5013 [hep-ph].
67. G. D. Kribs, T. S. Roy, J. Terning and K. M. Zurek, arXiv:0909.2034 [hep-ph].
68. S. Chang, G. D. Kribs, D. Tucker-Smith and N. Weiner, *Phys. Rev. D* **79**, 043513 (2009).
69. S. Chang, A. Pierce and N. Weiner, *Phys. Rev. D* **79**, 115011 (2009).
70. D. P. Finkbeiner and N. Weiner, *Phys. Rev. D* **76**, 083519 (2007).
71. R. Bernabei *et al.* [DAMA Collaboration], *Eur. Phys. J. C* **56**, 333 (2008).
72. P. Jean *et al.*, *Astron. Astrophys.* **407**, L55